J. Fluid Mech. (1994), *vol.* 266, *pp.* 1–32

An experimental investigation of concentrated suspension flows in a rectangular channel

By CHRISTOPHER J. KOH†, PHILIP HOOKHAM‡ AND L. G. LEAL

University of California, Santa Barbara, Department of Chemical and Nuclear Engineering, Santa Barbara, CA 93106, USA

(Received 21 March 1991 and in revised form 5 August 1993)

An experimental adaptation of the well-known laser-Doppler anemometry technique is developed for measuring the velocity and concentration profiles in concentrated suspension flows. To circumvent the problem of optical turbidity, the refractive indices of the solid and liquid phases are closely matched. The residual turbidity, owing to small mismatches of the refractive indices, as well as impurities in the particles, allows a Doppler signal to be detected when a particle passes through the scattering volume. By counting the number of Doppler signals in a period of time, the local volume fraction is also measured.

This new technique is utilized to study concentrated suspension flows in a rectangular channel. The general behaviour of the suspension is that the velocity profile is blunted while the concentration profile has a maximum near the centre. Comparisons are made with theoretical predictions based on the shear-induced particle migration theory.

1. Introduction

Most studies of the flow properties of suspensions of spherical particles have focused upon the development of theoretical or empirical formulae relating the bulk rheology (and especially the suspension viscosity) to the volume fraction of particles and/or to the magnitude of Brownian and colloidal forces, assuming that the concentration of particles remains uniform in space. It has been recognized for some time, however, that a number of mechanisms exist in the presence of flow that can lead to non-uniform concentrations even in the region away from any walls or flow boundaries. When this occurs, macroscopic measures of the resistance to flow (such as the volumetric flow rate for a given pressure gradient) will exhibit apparent non-Newtonian behaviour even if the suspension is sufficiently dilute and free of colloidal interaction forces that its constitutive behaviour is everywhere Newtonian, albeit with a viscosity that depends on the local volume fraction of particles.

One class of effects leading to non-uniform concentration distributions in simple shear flows are the so-called 'lateral migration' mechanisms that produce cross-stream motions of even single particles (cf. the review paper by Leal 1980). Among these, the best known are inertia-driven migration (responsible for the well-known Segré–Silberberg (1962, 1963) effect), migration due to deformation of particle shape (responsible for non-uniform concentrations in emulsions, and for the so-called

† Current address: Mobil E & P Technical Center, 1377 Midway Road, Dallas, TX 75244.
‡ Current address: California Research & Technology, 20943 Devonshire Street, Chatsworth, CA 93199.

Fahraeus–Lindquist (1931) effect of a 'clear fluid' region near the walls in the motion of whole blood), and migration due to non-Newtonian properties of the suspending liquid, studied first by Karnis & Mason (1967) and Gauthier, Goldsmith & Mason (1971). When these effects occur in a suspension in competition with Brownian motion (or any other mechanism that tends to restore the equilibrium state of uniform concentration on a finite timescale), the result will be non-uniform concentration profiles with a degree of non-uniformity that is flow-rate dependent.

More recently a second class of mechanisms has been discovered for the evolution of non-uniform concentration profiles which are a consequence of irreversible interactions between particles. This mechanism is believed to be responsible, in part, for the seemingly anomalous experimental observations of Karnis, Goldsmith and Mason (1966). By using hand-analysed cinematography, these researchers found that the velocity profiles of the particles for flow of a suspension of non-Brownian and non-colloidal spheres through a tube were increasingly blunted at the centre as either the particle size or the particle concentration was increased. Puzzling, however, was the fact that the particle concentrations, as determined by a direct count of tracer particles crossing a plane, was reported to be uniform. The first explicit recognition of the possibility of a cross-stream flux of particles owing solely to irreversible interaction effects seems to be due to Leighton & Acrivos (1987), who were motivated by apparently anomalous experimental findings of Gadala-Maria & Acrivos (1980). Indeed, by using scaling arguments, Leighton & Acrivos were able to derive a general expression for the 'diffusive flux' of particles in a unidirectional shearing flow. This expression was later adopted by Phillips *et al.* (1992) in the form

$$\frac{\partial \phi}{\partial t} + \nabla \cdot \boldsymbol{J} = 0 \quad \text{with} \quad \boldsymbol{J} = -K_c a^2(\phi^2 \nabla \dot{\gamma} + \phi \dot{\gamma} \nabla \phi) - K_\eta \dot{\gamma} \phi^2 \left(\frac{a^2}{\eta}\right) \frac{\mathrm{d}\eta}{\mathrm{d}\phi} \nabla \phi. \tag{1}$$

Here a is the particle radius, ϕ the local volume fraction of particles, $\dot{\gamma}$ the local shear rate, and η the suspension viscosity, while K_c and K_η are proportionality constants of order unity that must be obtained empirically. The two qualitative effects inherent in the expression for $\boldsymbol{J}$ are: first, that gradients of ϕ or $\dot{\gamma}$ will lead to an interaction frequency that increases in the direction of increasing $\dot{\gamma}$ or ϕ; and secondly, that gradients of ϕ are reflected in gradients of the suspension viscosity, thus leading to a greater drift velocity in the direction of smaller ϕ. A more detailed rationalization for the terms in this expression can be found in the original paper of Leighton & Acrivos (1987), or in later applications of this work such as Phillips *et al.* (1992). However, the presence of a ϕ^2 dependence signals the dominance of two-particle interactions in the mechanisms leading to the cross-stream particle flux. Since two-particle hydrodynamic interactions are known to be reversible in Stoke's flow, Leighton & Acrivos later suggested that particle roughness, leading to non-hydrodynamic interactions, may be the source of irreversibility required to produce a net lateral displacement via two-particle 'collisions'. Although roughness may well be a factor in some cases, it is now well known that the presence of even a weak perturbation to the two-particle motions due to a (distant) third particle may be enough to yield chaotic trajectories and an interaction that is irreversible on long timescales even for absolutely smooth particles.

In the periods both prior to, and after the landmark work of Leighton & Acrivos (1987), a number of authors have considered both new experiments and theory. On the experimental side, Kowalewski (1980) used ultrasound-Doppler anemometry to measure the velocity profile for concentrated suspensions of solid and liquid particles in tube flows. In the case of solid suspensions, she found that the blunting of the velocity profile can be characterized by the empirical formula $v = v_0(1-r^b)$, with b

increasing with the concentration of the suspension and the relative size of the particles. Although the ultrasonic experimental method is very useful, it cannot distinguish between particle and fluid velocities; the measured velocity profile is presumably a mass or volume averaged value. Clearly, no particle concentration data is possible via this technique. In later work, Kowalewski (1984, 1987) used an LDA technique to measure velocity profiles for suspensions of drops, and a light adsorption method to estimate the concentration profiles in flow through a tube. However, no additional data was observed on suspensions of solid spheres.

More recently, Hookham (1986) used a modified laser-Doppler technique to measure the velocity and concentration profiles for the flow of concentrated suspensions in a rectangular channel. He measured the Doppler signals from a trace fraction of the particles that were fluorescent-dyed and found that the velocity profiles were similar to the ones given by previous researchers (i.e. blunted near the centre). The degree of blunting was also found to increase as the bulk particle concentration or the particle size-to-gap ratio increased. By counting the number of fluorescent Doppler signals, he also found that there were more particles near the centreline of the channel so that the concentration profile had a maximum near the centre. However, the concentration data had a relatively large degree of scatter and could only provide a qualitative picture of the particle concentration distribution within the flow channel.

Finally, after the present experiments were completed,† two sets of researchers have reported data obtained via NMR imaging techniques, Sinton & Chow (1991) and Abbott *et al.* (1991). The former authors report velocity blunting, but no measurable non-uniformity of particle concentration. Abbott *et al.*'s (1991) measurements, on the other hand, were taken in a wide-gap Couette device and are thus not directly comparable to the present work, but do show a definite migration of particles toward the outer cylinder, namely from the region of highest shear-rates toward the lowest shear-rates in the flow system.

From a theoretical point of view, there have been three general approaches to studying the 'hydrodynamic diffusion' process. First, in the computational equivalent of an experiment, Nott & Brady (1993) have recently carried out dynamic simulations of pressure-driven flow of a suspension of non-Brownian particles in a two-dimensional channel, for a monolayer of identical spherical particles. These simulations demonstrate the gradual migration of particles toward the centre of the channel, leading to a concentration maximum near the centreline, and a blunting of the particle velocity profiles, in at least qualitative agreement with the experimental results reported below. Secondly, following the lead of earlier studies by Jenkins & McTigue (1990). Nott & Brady (1993) proposed a model for concentrated suspensions in the same paper, in which the concept of a hydrodynamic temperature was used as a measure of the intensity of the velocity fluctuations of the particles. This model produces results for channel flow that agree with the authors' numerical simulation results. Thirdly, Phillips *et al.* (1992) have adapted the scaling arguments of Leighton & Acrivos (1987), together with an empirical relationship between the suspension viscosity and the particle concentration, to obtain predictions using the generalized diffusion equation (1).

In the case of Couette flows, Phillips *et al.* (1992) find that particle migration causes ϕ to increase from the inner, rotating cylinder to the outer, stationary cylinder. These

† After submitting the manuscript for this paper and having it reviewed, we postponed resubmitting the revised paper to provide an opportunity to repeat many of the experiments and thus provide additional confidence in their accuracy. This was motivated by the fact that the measured particle velocities suggest serious deficiencies in current theories.

predicted concentration profiles agree very well with concentration profiles obtained from NMR studies of Couette flows for average particle concentrations of 50% and 55%. In addition, their calculations predict that the velocity decreases rapidly from the inner cylinder so that there is a relatively large region of almost stagnant suspension near the outer cylinder.

For axisymmetric Poiseuille flows, Phillips *et al.* (1992) predict that the particles tend to migrate toward the centreline so that the particle concentration is a maximum at the centre and a minimum at the walls. Since the viscosity of the suspension increases as a function of particle concentration, this concentration profile leads to a velocity profile that is flattened near the centre. This is in general agreement with the experimental results of Karnis *et al.* (1966) for the velocity profile (these authors did not find any non-uniformity in concentration), and with the simulation results of Nott & Brady (1993).

The present paper describes experimental results obtained for flow of a suspension of non-Brownian spherical particles in a two-dimensional channel flow. The objectives, for this first study from our laboratory, are simply to measure the concentration and velocity profiles for the particles for mean concentrations in the range $0.1 \leqslant \phi \leqslant 0.3$. A secondary objective is to demonstrate the applicability of straightforward LDV measurements for this purpose, when applied to a suspension in which there is a match of refractive indices between the particles and the suspended particles.

2. Experimental technique

As indicated in the previous section, there are various experimental techniques available for the study of the motion of concentrated suspension flows. However, all of these suffer from one or more deficiencies. For example, the cinematography of Karnis *et al.* (1966) is extremely labour intensive and cannot be expected to provide very accurate data (e.g. the uniform concentration profiles reported by these authors may be a consequence of experimental imprecision). The ultrasound-Doppler anemometry technique of Kowalewski (1980) cannot distinguish between the velocity of the fluid and the particles, and cannot provide a measurement of the concentration of the suspension. McMahon & Parker (1975) used a microwave-Doppler technique to measure suspension velocity in a tube flow. However, owing to the relatively long wavelengths of microwave, the spatial resolution of their technique is not sufficient to provide local velocity data. Finally, Sinton & Chow (1991) and Abbott *et al.* (1991) have used NMR imaging techniques to study suspension flows. These techniques actually measure the motion and local volume fraction of the suspending fluid. Though they should be capable of detecting non-uniform concentrations and of yielding fluid velocity measurements, the studies to date have not always obtained results that agree with other investigators, and there are limitations both in spatial and (especially) temporal resolution (not to mention a rather high capital equipment cost).

The experimental method that we employ here is laser-Doppler anemometry (LDA). This technique was chosen over other experimental techniques for various reasons. First of all, it is capable of measuring velocity accurately with comparatively good spatial resolution without physically disturbing the flow. Secondly, as we shall see, the LDA technique can be easily adapted to provide a measure of the particle concentration with the same spatial resolution. Thirdly, though we have not utilized additional capabilities here, the LDA technique can also be adapted (through use of optically distinct tracer particles) to provide an independent measurement of the suspending fluid velocity, and the instantaneous data can also be used to study the statistics of

particle velocity fluctuations instead of just the mean (or time averaged) velocities. Finally, LDA is now widely available and an equivalent system can be easily set up in most laboratories.

In the remainder of this section we discuss the fundamental principles of the experimental technique. Subsequently, we will discuss the particular details of the experimental set-up in our laboratory for the study of concentrated suspension flows. For a detailed account of the principles and operation of LDA see, for example, Drain (1980), and Durani & Greated (1977). It may be noted that a similar experimental apparatus to that reported here was used by Hookham (1986) to study suspension flows; however, he obtained Doppler signals from fluorescent dye-coated particles.

In order to study high-concentration suspensions using an optical experiment such as LDA, we must overcome the problem of optical turbidity, which is generally absent in the application of LDA to a pure fluid flow. To circumvent this problem, it is imperative that we minimize the optical turbidity of the suspension – through refractive index matching of the suspending and particulate phases. As we subsequently show, this was a crucial step in our LDA measurements of suspension flow.

3. Refractive index match

Optical turbidity presents a major problem in the application of LDA to suspension flow, especially at high particle concentrations where the intensity of the laser beams is strongly attenuated. Since the strength of the Doppler signal is proportional to the intensity of the laser beams, attenuation of beam intensity can lead to lower signal-to-noise ratios (noise sources include random shot noise of the photomultiplier tube, spurious signals due to stray laser light, random noise generated by post-photomultiplier tube electronics, etc., cf. Arian 1978). Beyond the loss of intensity, multiple scattering can also 'deflect' the laser beam from its original optical path; this can lead to ambiguity in the position of the measurement volume. Fortunately, all of these detrimental effects can be minimized by matching the refractive indices of the particles and the suspending liquid.

Currently, we are interested in studying suspensions of neutrally buoyant spherical particles. The constraints of simultaneously matching the density and index of refraction of the particles and suspending fluid limit the type of particles that can be used in the experiment. The most important requirement is that they are transparent (i.e. the imaginary part of the refractive index has to be negligible so that light is not absorbed). Furthermore, the particles have to be spherical and in the density range of the suspending fluid. The particles we chose are monodispersed polystyrene (with divinylbenzene cross-linkage) particles with nominal diameters of 30, 50 and 89 μm, respectively. These particles, supplied by Duolite and Bio-Rad, are normally used for ion-exchange chromatography and therefore are available in bulk quantities commercially. Figure 1 shows a typical particle size distribution for these particles (here, data is shown for the nominally 30 μm particles).

As mentioned above, it is necessary to match not only the refractive indices but also the densities of the particulate and suspending phases. This dictates the use of a three-component suspending fluid so that the density and the refractive index can be adjusted independently. For the polystyrene particles, the refractive index is approximately 1.6 and the density is 1.05 g cm^{-3}. The liquids chosen for the suspending fluid must have properties 'bracketing' these values. The densities of most liquids are around the value of 1.05 g cm^{-3}. However, only a small number of liquids, such as the liquid phase of various aromatic compounds, have refractive index values as high as 1.6. Specifically,

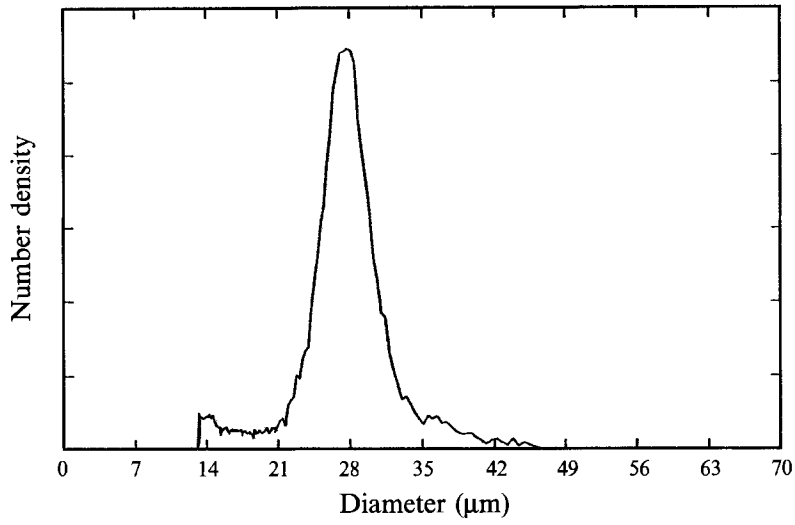

FIGURE 1. Particle size distribution curve for the nominally 30 μm particles.

	Viscosity (c*P*)	Density (g cm^{-3})
1-Chloronaphthalene		
16.0 °C	3.79	—
20.0 °C	3.42	1.191
24.0 °C	3.13	—
1-Methylnaphthalene		
16.0 °C	3.70	—
20.0 °C	3.29	1.017
24.0 °C	2.97	—
UCON oil 75-H-90000		
16.0 °C	6.89×10^4	—
20.0 °C	5.11×10^4	1.094
24.0 °C	4.18×10^4	—
Suspending liquid		
16.0 °C	148	—
20.0 °C	124	1.052
24.0 °C	106	—

TABLE 1. Viscosities and densities of the fluids used in the experiment at various temperatures

we chose the following liquids, 1-methylnaphthalene (Aldrich catalogue number M5,680-8), 1-chloronaphthalene (Aldrich C5,765-0) and UCON-oil (polyalkylene-glycol, Union Carbide product number 75-H-90,000), to constitute the liquid phase. The first two components are aromatic compounds with a relatively high refractive index. The UCON-oil is chosen because it is miscible with the naphthalenes and has a density and refractive index that can provide the required properties for this three-component liquid. The densities and viscosities of these liquids were measured using a pycnometer and various sizes of Cannon–Fenske viscometer, respectively. The values are reported in table 1.

To match the refractive indices of the two phases, several effects must be considered. First, the refractive index of the liquid used in these experiments depends strongly on temperature, as seen in figure 2. These refractive index values were measured using a

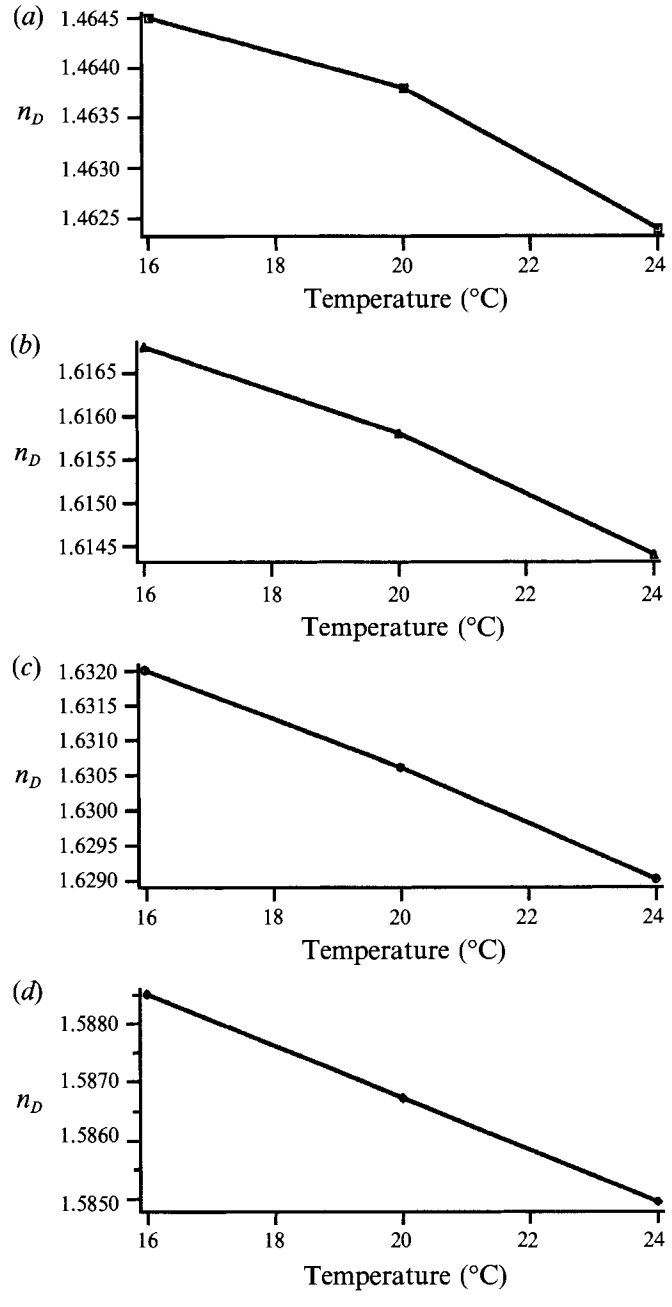

FIGURE 2. Temperature dependence of refractive indices. (*a*) UCON oil 75-H-90000; (*b*) 1-methylnaphthalene; (*c*) 1-chloronaphthalene; (*d*) suspending solution.

Bausch & Lomb refractometer in conjunction with a Neslab temperature control unit. The temperature coefficient of the three-component solution is about -4.5×10^{-4} °C. On the other hand, the temperature dependence of the index of refraction of the polystyrene particles is -1.42×10^{-4} °C (Timmermans 1965). Thus, the degree to which the refractive indices can be matched depends on how well the temperature of the suspension can be controlled during the experiment.

The second factor is the wavelength dependence of the refractive index. It is crucial

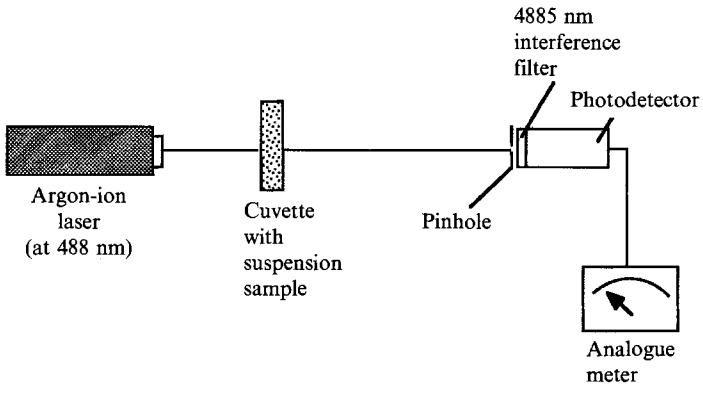

FIGURE 3. Schematic diagram of turbidity experiment.

that the refractive indices be matched at the particular laser wavelength used in the experiment, namely 488 nm. Thus, it is not sufficient to simply match the refractive indices of the two phases by selecting the 'clearest' suspension with the naked eye under ambient lighting. A more accurate and systematic method is necessary.

As far as we know, there is no known method for measuring the refractive index of small particles accurately and conveniently. Thus, it is not possible to measure the refractive index of the polystyrene particles first, then find a solution with a composition that has the same refractive index. Nouri, Whitelaw & Yianneskis (1986) demonstrated an ingenious way of matching the refractive indices of Diakon particles and a solution of tetraline and turpentine. They aimed a laser beam into the solution containing a large Diakon rod. By varying the composition of the solution (thus varying its refractive index), the laser beam passed through the system with different degrees of deflection. The point of perfect match was ascertained when the beam passed through the system without any deflection.

Unfortunately, we do not possess a bulk polystyrene sample that has the same molecular structure (hence the same refractive index) as the polystyrene–divinylbenzene particles. Thus, we were not able to match the refractive indices at the specific laser wavelength using the experimental procedure described above. However, Conaghan & Rosen (1972) developed a theory that quantifies the degree of light scattering in a suspension as a function of the refractive indices of the two phases. The transmittance of light through a sample of thickness x is defined as:

$$T \equiv \frac{I}{I_0} = \mathrm{e}^{-\tau x}, \tag{2}$$

where I_0 is the intensity of the incident light and I is the intensity of the transmitted light. For a perfectly matched system, $T = 1$; otherwise, $T < 1$.

The turbidity, τ, is given by

$$\tau = \frac{3\phi K}{2d_p}, \tag{3}$$

where ϕ is the particle volume fraction, d_p is the particle diameter and K is the scattering coefficient. Normally, it is necessary to solve Maxwell's equation to obtain K. However, for large particles ($d_p \gg \lambda$, the wavelength of the incident light), Van de Hulst (1957) derived the following relationship:

$$K = 2 - \frac{4}{\rho}\sin\rho + \frac{4}{\rho}(1 - \cos\rho), \tag{4}$$

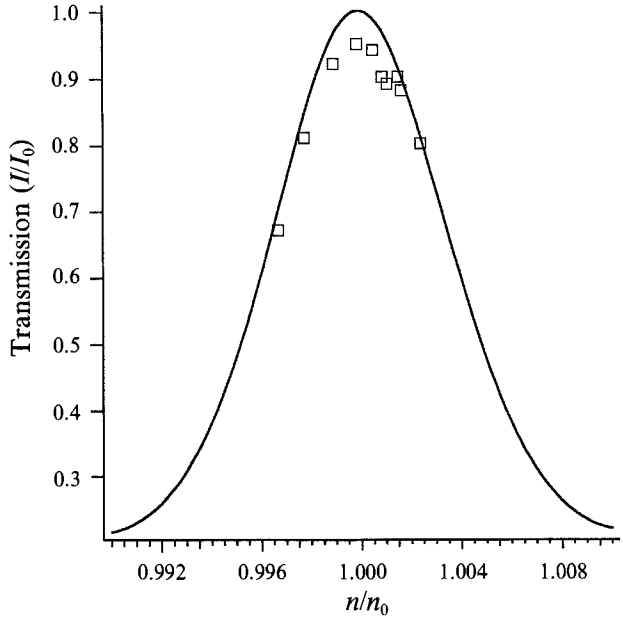

FIGURE 4. □, Experimental results from a typical turbidity experiment: $\phi_{bulk} = 0.1\,\%$, $d_p = 320$ μm, $\lambda = 488$ nm, and comparison with —, theoretical transmittance curve ($n_0 = 1.5867$). $T = 20.0 \pm 0.4$ °C.

where
$$\rho = \frac{2\pi d_p n_0}{\lambda}|m-1| \tag{5}$$

and
$$m = \frac{n}{n_0}.$$

Here, n_0 and n are the refractive indices of the particle and the suspending fluid, respectively.

We now discuss an experimental procedure that measures the transmittance of suspensions. Figure 3 shows the schematic diagram of the experiment. By measuring the intensity of the laser after it passes through the suspension, we can calculate the transmittance. In order to take into account the inherent turbidity and light absorbance of the solution, I_0 is actually the transmitted intensity of the laser after it passes through the particle-free solution. Figure 4 shows the experimental results for $\Phi_{bulk} = 0.1\,\%$, $d_p = 30$ μm, $\lambda = 488$ nm and various solution refractive indices.

To find the refractive index of the polystyrene particles (n_0), we choose n_0 such that the quantity
$$E \equiv \sum \left[T_e\left(\frac{n}{n_0}\right) - T_t\left(\frac{n}{n_0}\right) \right]^2 \tag{6}$$
is minimized. Here, $T_e(n/n_0)$ is the experimental transmittance, $T_t(n/n_0)$ is the theoretical transmittance and n is the refractive index of the solution. As expected, the maximum transmittance occurs at n_0. The exact value of n_0 that minimized E for the present system was 1.5867 (at 20 °C). We have found empirically that the composition (by weight) of the liquid with this refractive index and also a density equal to the particles is approximately 67.7 % 1-methylnaphthalene, 10.4 % 1-chloronaphthalene and 21.9 % UCON-oil.

Using this value of n_0, a theoretical transmittance curve has been plotted against the experimental data in figure 4 for comparison. We can see that the experimental data fit the theoretical prediction quite well. It is clear, however, that $T_{e,max} < T_{t,max} = 1$. This is presumably due to a small but finite mismatch of the refractive indices associated primarily with localized trace amounts of impurities within the particles. In fact, it is this residual turbidity that allows a particle to produce a Doppler signal when it passes through the scattering volume.

As stated earlier, the temperature coefficients of the refractive index of the solution and the polystyrene particles are different. Therefore, even when the refractive indices of the two phases are matched (i.e. $n/n_0 = 1$) at a specific temperature, say 20 °C, n/n_0 will deviate from unity as temperature fluctuates during the course of the experiment. If the temperature is controlled to within ± 0.5 °C, then

$$n = 1.5867 \pm 0.0002, \tag{7}$$

$$n_0 = 1.5867 \pm 0.00007. \tag{8}$$

As a result, the variation in m becomes

$$m = 1.0 \pm 8 \times 10^{-5}. \tag{9}$$

Using equations (2) and (3), and assuming $\phi = 0.3$ and $x = 1.0$ mm (a typical gap width of the flow device), we find that the transmittance is reduced from unity to 0.99. Of course, the actual transmittance will be lower than this theoretical figure owing to impurities or optical imperfections in the particles. In practice, we found that it was sufficient to control the temperature of the suspension to within ± 1 °C.

As we have shown, the refractive indices of the two phases were matched at $n = 1.5867$ at 20 °C. However, the turbidity of the suspension slowly increased over a period of several days. In fact, the refractive index of the filtrate (i.e. the suspending liquid) of an old suspension decreased with the age of the suspension. We believe that the polystyrene–divinylbenzene particles selectively absorb the lower molecular weight 1-methylnaphthalene and 1-chloronaphthalene, thus slowly changing the refractive indices of both the suspending liquid and the particles. Consequently, all experiments were performed with fresh suspensions within a five-hour period, during which the turbidity of the suspension does not increase significantly.

Finally, there are a number of issues that arise from the fact that, in the context of LDA, a refractive-index-matched suspension of (relatively) large particles is somewhat different from a fluid seeded with a large number of submicron particles (as in many LDA measurements of fluid flow). In the present case, the particle size is of the order of the measurement volume so that the Doppler signal almost always comes from a single particle. On the other hand, in the usual case, many small particles could be present in the measurement volume and they all contribute to the signal both coherently and non-coherently (see Drain 1972 for a more detailed discussion). We presume in the data analysis, that the LDA signal comes from light scattered due to slight refractive index imperfections that are also apparent in figure 4. As we shall see, the particle concentration is found by measuring an average time between bursts, assuming that each burst corresponds to a single particle, and that the average mismatch in refractive index is the same for all particles. It is, of course, not obvious whether the mean refractive index mismatch is a consequence of a relatively uniform fluctuation in the refractive index throughout the particle, or of a single localized region of mismatch (a defect). However, the form of the LDA burst appears very similar to what we would expect for a single particle that is smaller than the scattering volume. This suggests that the scattering may occur from localized optical defects in

the particles which are separated by distances of the order of the lengthscale of the scattering volume (i.e. there are $O(1)$ scattering centres per particle). Obviously, however, it is not feasible to optically characterize individual particles, and it is possible that some particles may be sufficiently free of optical imperfections as to be 'invisible' in the scattering experiment, or that others may contain more than one distinct scattering centre, and thus be counted twice. In any case, the data reported represents averages over many scattering events, and none of these uncertainties should influence the relative concentrations reported (the probability of non-idealities in the optical properties of the particles is independent of position by assumption). Indeed, since the experiment is capable only of obtaining relative concentrations, as we shall see, specific values at any point are only obtained by normalization and this process will wipe out any bias in the data that is independent of position in the channel.

4. Experimental set-up and data analysis

The experimental set-up is shown in figure 5. The whole system is secured on a pneumatically elevated optical table (Newport Research MST-48) for isolation from vibration. The laser is a Spectra-Physics model 165 argon ion laser operating at 488 nm. All optical elements are coated with anti-reflective coatings (for lenses and optical windows) or maximum reflection coatings (for mirrors), which are optimized at the laser wavelength. After the laser beam exits the laser cavity, it is deflected by various mirrors (e_1 and e_2) to an appropriate position for entrance into the beam splitter (element e_3), which produces two equal intensity laser beams at the output end. Element e_4, an integral optical element consisting of two mirrors and a reflective prism, allows for easy adjustment of the beam separation through the movement of the prism along the laser beams' direction of propagation, as well as additional degrees of freedom for proper beam alignment. The beams are then focused down to a Gaussian diffraction-limited radius of 9.2 μm within the flow device by a 120.8 mm focal length plano-convex lens. The beam crossing angle is limited by lens astigmatism through the beam separation distance, with a maximum value of 26.6° in air (17.2° for the suspension mixtures) occurring for a beam separation of approximately 60 mm. Scattered light is collected by a camera lens (Nikon) which has a focal length of 50 mm (operating at *f*5.6), and focused onto a 50 μm diameter pinhole placed in front of the photomultiplier tube (Hammamatsu model R1617 operating at a potential of 0.85 kV). The purpose of the pinhole is two-fold; it reduces the size of the effective measuring volume, and prevents stray light from reaching the photomultiplier tube. Signal processing is performed by a TSI Model 1980B Counter Processor, which is interfaced with a microcomputer (PC-AT) for data acquisition and reduction.

Since a counter-type signal processor is used to determine the frequency of each Doppler burst, the measuring volume size depends upon the focusing and power of the illuminating laser beams, the scattering properties of the particles, the efficiency of light collection by the receiving lens, as well as sensitivity and amplification of the processing electronics (Adrian 1978). For these experiments all of the above are known or can be estimated, except for the particle scattering properties, which are ambiguous because Mie scattering theory requires knowledge of the refractive index of the particles relative to the surrounding fluid as well as the size of the light scattering region (Adrian & Earley 1976).

Instead, the dimensions of the probe volume seen by the detector will be reported. This region is defined as the intersection of the pinhole image through the collection lens with the ellipsoidal region defined by the focused Gaussian beam intersection that

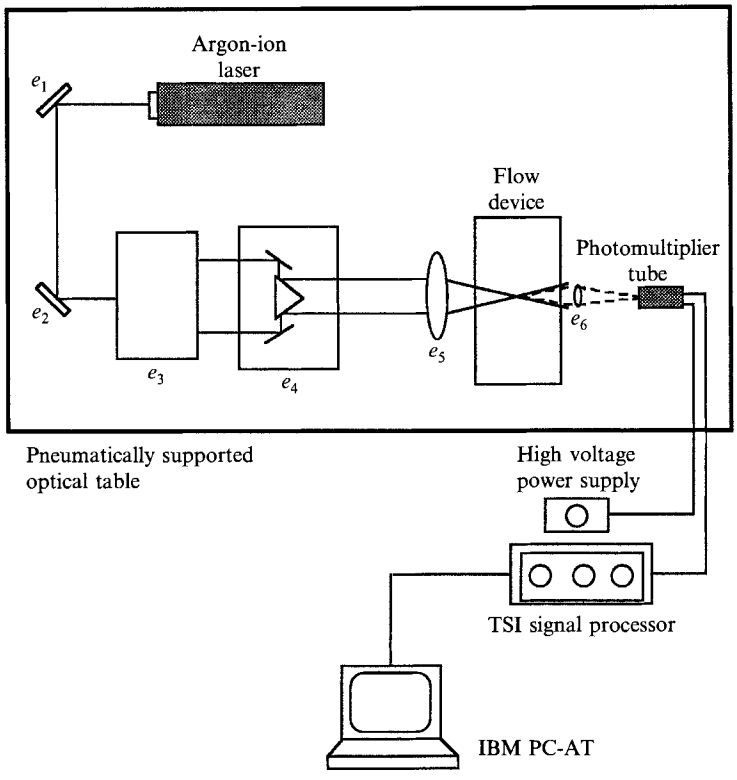

FIGURE 5. Schematic diagram of LDA experiment.

possesses irradiance that is e^{-2} of its maximum value (the irradiance at the intersection of two beams along their axes). The major axes of this ellipsoidal volume calculated from the diffraction limited beam radius and the crossing angle of the two illuminating beams given above are 121 μm, 18.5 μm, and 18.3 μm along the optical axis, normal to the optical axis and in the plane containing the two beams, and normal to the optical axis and lying in the plane parallel to the optical table, respectively. Since the collection optics rest at an angle of about 15° in the plane coincident with the optical table, and the collection lens relative magnification is approximately 3, the major axes of the region as seen at the detector are then 64.7 μm, 17.2 μm, and 16.6 μm (corresponding to the directions above), respectively.

4.1. *Calculation of average particle velocity and volume fraction*

In a typical experiment, 500–1000 data points were obtained for each average velocity or concentration value reported at a point in the flow channel. For each Doppler signal processed by the signal processor, the computer receives three pieces of information: n_c, t_s and t_d. n_c is the number of cycles in the Doppler burst, t_s is the duration of this signal, and t_d is the time between the current and the previous signal. The Doppler frequency is simply given by

$$f_{Doppler} = \frac{n_c}{t_s}. \tag{10}$$

From LDA theory, the Doppler frequency can be converted into the z-component of the velocity as follows

$$v_z(x) = \frac{\lambda}{2\sin\frac{1}{2}\alpha} f_{Doppler}, \tag{11}$$

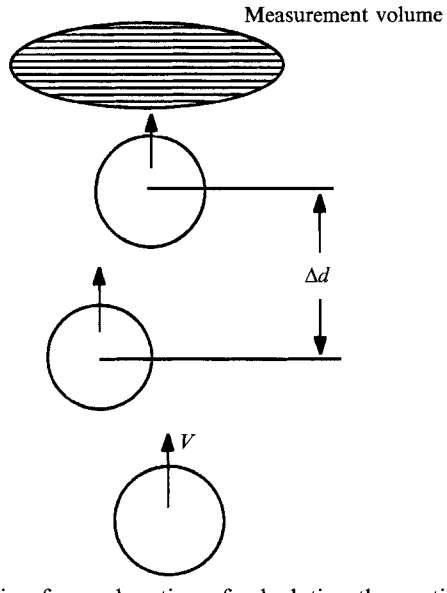

FIGURE 6. Illustration for explanation of calculating the particle volume fraction.

where x denotes a specific point in the flow device. Using $\lambda = 0.488$ μm and $\alpha = 26.6°$, we obtain

$$v_z \text{mm/s} = 1.06 f_{Doppler} \text{kHz}. \tag{12}$$

The average local velocity at a point x is then given by

$$\overline{v_z(x)} = \frac{\sum_{i=1}^{N} v_{zi}}{N}, \tag{13}$$

and the standard deviation of the velocity is also calculated

$$\sigma_{v_z} = \frac{\sum_{i=1}^{N} [(v_{zi} - \overline{v_z})^2]^{\frac{1}{2}}}{(N-1)}. \tag{14}$$

To obtain the particle volume fraction, recall that the size of the measurement volume is of the order of a particle, as shown in figure 6. A local (instantaneous) estimate of the volume fraction of particles is thus proportional to

$$C(x) \sim \frac{V_p}{A_{mv} \Delta d}. \tag{15}$$

Here, A_{mv} is the cross-sectional area of the measurement volume, V_p is the particle volume, and Δd is the instantaneous separation between any two successive particles which pass through the scattering volume, i.e.

$$\Delta d = V_z t_d, \tag{16}$$

where V_z is the instantaneous particle velocity (either the velocity of one of the particles, or the average of the pair), and t_d is the time between LDA bursts. It is assumed, in writing (15) that the change in particle concentration across the scattering volume is negligible. The average concentration is thus

$$\overline{C(x)} \cong \frac{1}{N} \sum_{i=1}^{N} C_i(x), \tag{17}$$

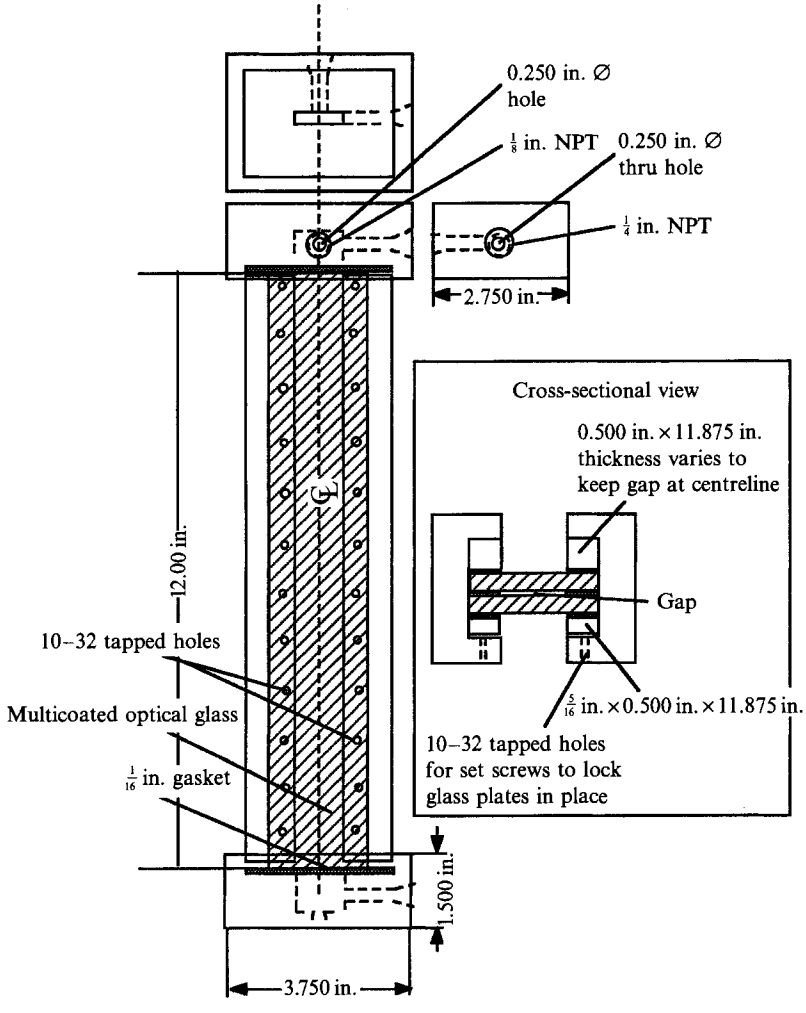

FIGURE 7. Schematic diagram of flow channel.

$$\text{or} \qquad \approx \frac{1}{A_{mv}} \frac{1}{(V_z t_d)}, \tag{18}$$

$$\text{where} \qquad \overline{V_z t_d} = \frac{\sum_{i=1}^{N} (V_z t_d)_i}{N}. \tag{19}$$

There are a number of uncertainties in the measurements that require us to consider $\overline{C}$ as a relative concentration rather than an absolute value. Some of these were mentioned earlier, e.g. variability in the optical properties from particle to particle which means that some may not register a sufficiently strong scattering signal to be registered even though they pass directly through the scattering volume. Others, like our inability to provide a precise value for A_{mv} are evident. Thus, assuming that the measurement uncertainties yield the same fractional change in the relative concentration, $\overline{C}$, the actual volume fraction of particles can be expressed in the form

$$\overline{\phi}(x) \equiv \frac{kV_p}{A_{mv}(\overline{V_z t_d})} = \frac{k'}{\overline{V_z t_d}}, \tag{20}$$

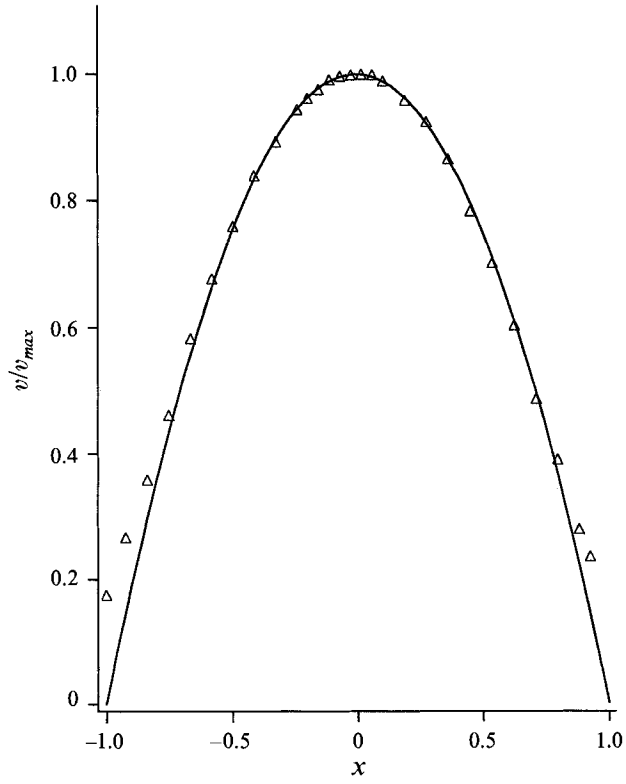

FIGURE 8. Comparison between △, experimental data and —, parabolic velocity profile. V_{max} = 31.5 mm s^{-1} and channel gap width = 0.062 in.

where k (and thus k') is a constant of proportionality that must be determined via some type of normalizing condition. In the present work, k' is determined by satisfying the condition

$$\phi_{bulk} = \int \bar{\phi}\, \mathrm{d}x \Big/ \int \mathrm{d}x. \tag{21}$$

It should be noted, however, that it is more accurate, in principle, to choose k' so that the volume flux of particles is equal to the inlet value rather than ϕ being equated to ϕ_{bulk}, and this is the approach that is currently being utilized in our laboratory. In any case, there is a significant uncertainty in the quantitative values of $\bar{\phi}$, though the qualitative trends are clearly established by the present experiments.

4.2. *Test of the experimental system*

In order to ascertain that the LDA system and the data collection system were functioning properly, the velocity profiles were measured for the rectangular channel flow of a Newtonian fluid (water). The flow channel gap width for these measurements was 1570 μm, and the channel aspect ratio was 1:16. Figure 7 shows a schematic of the flow channel. The details of the flow system are explained in §5. The Doppler signals for this test were obtained from 5 μm seeding particles. Figure 8 shows an experimental profile compared to a theoretical (parabolic) profile at the higher of the two pump speeds used for the suspension flow experiments. The velocity data is non-dimensionalized with the corresponding velocity at the centreline of the flow channel (i.e. the maximum velocity). In general, there is good agreement between the experimental data and the expected parabolic profile. However, we can see that the

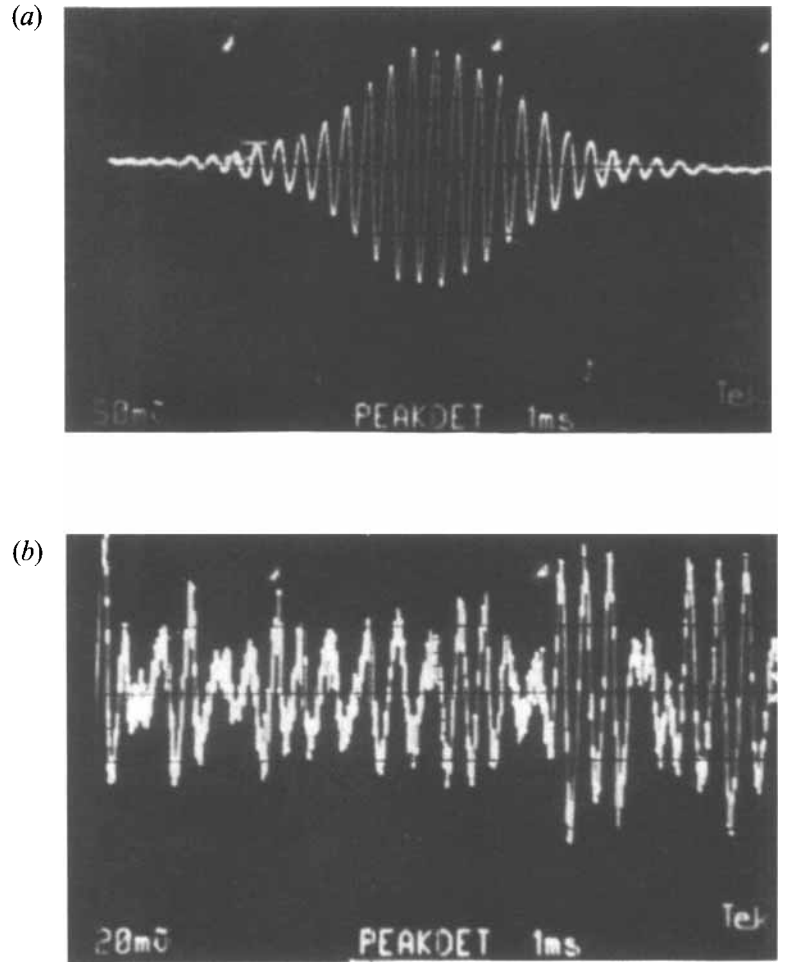

FIGURE 9. A comparison of oscilloscope traces (*a*) obtained from a refractive-index-matched suspension, with (*b*) the trace for a suspension without index matching. Traces at low sweep rate.

measured velocities are somewhat higher than the theoretical values near the walls. We can offer three possible explanations for this observation. First, the signal to noise ratio near the walls is lower owing to laser light reflected by the glass walls. This causes extraneous laser light to enter the receiving optics, thus increasing the noise level. Secondly, and more importantly, the TSI signal processor is equipped with a high-pass filter to eliminate the d.c. (low frequency) part of the signal. This filter eliminates frequencies below 1 kHz, which corresponds to a velocity of approximately 1 mm s^{-1}. The velocity near the wall is the lowest and the velocity gradient is the highest. Since the low-frequency (velocity) signals are eliminated electronically, only the high-frequency velocity signals are processed. Consequently, the average velocity obtained at a point near the wall is biased toward a higher value. (Although this problem can be resolved by using a Bragg cell to shift the frequency of one of the laser beams (cf. Durani & Greated 1977), the present experimental set-up was not equipped with a Bragg cell.) Finally, there is a natural upward bias due to the finite size of the scattering volume compared to the channel width.

As discussed above, we matched the refractive indices of the suspending and

particulate phases to reduce multiple scattering of the laser light. The exact quantitative difference between the Doppler signals obtained from suspensions with or without refractive index matching is impossible to predict. However, there are easily observed qualitative differences between the two cases. Figure 9 shows a comparison between a typical Doppler signal from a refractive-index-matched suspension as observed from a storage oscilloscope, and the Doppler signal from a suspension whose refractive indices were not matched. The bulk volume fraction of the suspension is 15%. For the latter case, the refractive index of the suspending fluid solution is 1.5858 (recall that the refractive index of the particles is 1.5867). The top trace shows a single Doppler burst that is free of noise and has a well-defined envelope. The signal without refractive index match does not have a well-defined envelope and there is a considerable level of high-frequency noise present.

5. Procedures and experimental conditions

In this section, we discuss the procedure for the operation of the experiments. Figure 7 shows the detailed dimensions of the flow channel as well as a schematic diagram of its cross-section. The optical quality Pyrex glass walls (available from Rolyn Optics, West Covina, California) were coated with a broadband multilayer dielectric coating and have a refractive index of 1.474. Besides the glass, the flow channel is made of black anodized aluminium (the black anodization reduces reflection of stray laser light). The precise gap width of the flow channel is determined by the thickness of the Lucite spacers, machined to within ± 0.001 inch. Two sets of twelve set screws were used to secure the glass plates to the aluminium pieces and to provide pressure to seal the two sides of the channel. To seal the top and bottom of the flow channel, rubber gaskets ($\frac{1}{16}$ inch thickness) were placed in between the top and bottom of the flow channel and the exit and entry blocks, respectively. The exit and entry blocks have openings so that thermocouples can be placed inside to monitor the temperature of the suspension.

The flow was produced by a Harvard Apparatus model 951 infusion-withdrawal pump fitted with a pair of 50 cm^3 precision-bore Robb infusion glass syringes. The flow system is closed-loop with one syringe pumping into the channel at any instant, while the output from the channel is simultaneously withdrawn into the other syringe. All the connection tubings are Teflon-coated to provide chemical inertness. The flow is (nearly) continuous in time with only a brief interruption when the pump reverses (and thus reverses the role of the two syringes). A reservoir is located between the outlet of the pump and the inlet to the channel in which the suspension is constantly stirred with a magnetic stirrer for the duration of the experiment.

For a typical experiment, the suspension was prepared by mixing the necessary amount of particles (depending on the desired bulk particle volume fraction of the suspension) in the liquid. Approximately 150 ml of suspension is required for the capacity of the overall flow system. The suspension was stirred manually to assure good mixing. It is then allowed to stand for 15–45 min so that any bubbles present in the mixture rise to the top. Since the turbidity of the suspension increases with time, as explained earlier, the suspension is discarded after about 4 h of experimentation.

6. Experimental results and discussion

To explore different possible phenomena associated with this problem, we have performed experiments for a range of values of the various important dimensionless parameters, namely, the bulk particle concentration (ϕ_{bulk}), the particle size to gap

Experiment	κ	Φ	Re_p
160	0.010	0.10	4.0×10^{-3}
158	0.010	0.10	2.0×10^{-3}
215	0.010	0.20	4.0×10^{-3}
217	0.010	0.20	2.0×10^{-3}
172	0.010	0.30	2.0×10^{-3}
186	0.019	0.10	4.0×10^{-3}
187	0.019	0.10	2.0×10^{-3}
191	0.019	0.20	4.0×10^{-3}
189	0.019	0.20	2.0×10^{-3}
194	0.019	0.30	4.0×10^{-3}
192	0.019	0.30	2.0×10^{-3}
199	0.032	0.10	6.6×10^{-3}
198	0.032	0.10	3.3×10^{-3}
204	0.032	0.20	6.6×10^{-3}
202	0.032	0.20	3.3×10^{-3}
207	0.032	0.30	6.6×10^{-3}
205	0.032	0.30	3.3×10^{-3}
246	0.057	0.10	1.2×10^{-2}
245	0.057	0.10	5.9×10^{-3}
224	0.057	0.20	1.2×10^{-2}
223	0.057	0.20	5.9×10^{-3}
226	0.057	0.30	5.9×10^{-3}

TABLE 2. List of experiments performed

ratio (κ), and the particle Reynolds number. These parameters are defined in the present study as follows:

$$\phi_{bulk} \equiv \frac{\text{particle volume}}{\text{particle} + \text{liquid volume}}, \tag{22}$$

$$\kappa \equiv \frac{a}{d}, \tag{23}$$

$$Re_p \equiv \frac{v_{n,0} \rho a}{\mu_{liquid}}. \tag{24}$$

Here, a is the radius of the particle, d is the gap width of the flow channel, $v_{n,0}$ is the centreline (maximum) velocity of a Newtonian fluid at the same volumetric flowrate, ρ is the density of the suspending liquid, and μ_{liquid} is the viscosity of the suspending liquid. The Reynolds number of the overall channel flow (Re) is simply given by

$$Re = \frac{Re_p}{\kappa}. \tag{25}$$

In the present work, two different volumetric flowrates were used, corresponding to Newtonian centreline velocities of 1.58 cm s^{-1} and 3.16 cm s^{-1}. The channel width was chosen as either 785 μm or 1570 μm, and the particles were 30, 50 and 89 μm in diameter. Finally, three different bulk concentrations were considered, $\phi_{bulk} = 0.1$, 0.2 and 0.3, respectively. A complete list of all combinations of experimental conditions that were used is given in terms of κ, ϕ_{bulk} and Re_p in table 2. All of the data reported here were obtained at a point approximately 12.7 cm from the entrance of the flow channel. Comparisons with data at 7.6 cm, and also at 17.8 cm from the entry, showed

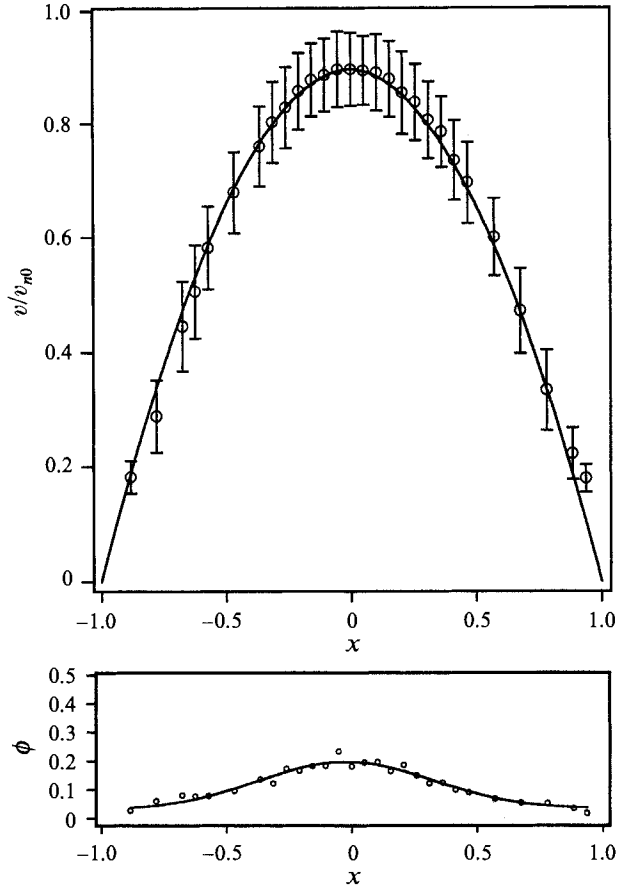

FIGURE 10. Velocity and concentration profiles for experiment 158 (see table 1): ○, data points; —, curve fits to data (see text); I, standard deviation for velocity data. $Re_p = 2.0 \times 10^{-3}$; $\kappa = 0.010$; $\phi_{bulk} = 0.10$; $b = 1.90$.

no changes within experimental error, and thus, in the absence of other information, we would suppose that our data represents the steady, fully developed velocity and concentration profiles. It should be noted, however, that recent estimates of the required channel length to achieve steady state, due to Nott & Brady (1993), would suggest that the data for the smallest κ value, $\kappa = 0.01$, may not be fully developed after all. Rather, their estimate for this particular case suggests that the channel would have needed to be 2500 times the half-width in length to achieve steady state, so that the profile comparisons we made in this case may actually have been too close together to have allowed us to discern a measurable change. Thus, it is possible that the results obtained for this specific case were not fully developed, though we believe that all other cases do represent the fully developed case.

The experimental results obtained in the present study are contained in the profiles of particle velocity and particle concentration that are presented in figures 10–21. These data are for the lower of the two flowrates that were used. Corresponding data for the higher flowrate is contained in Koh (1991). Though differing in minor detail, it is qualitatively indistinguishable from the data in figures 10–21, and mainly serves to corroborate the assumption that the particle Reynolds number was sufficiently small in our experiments that inertial migration is not a factor.

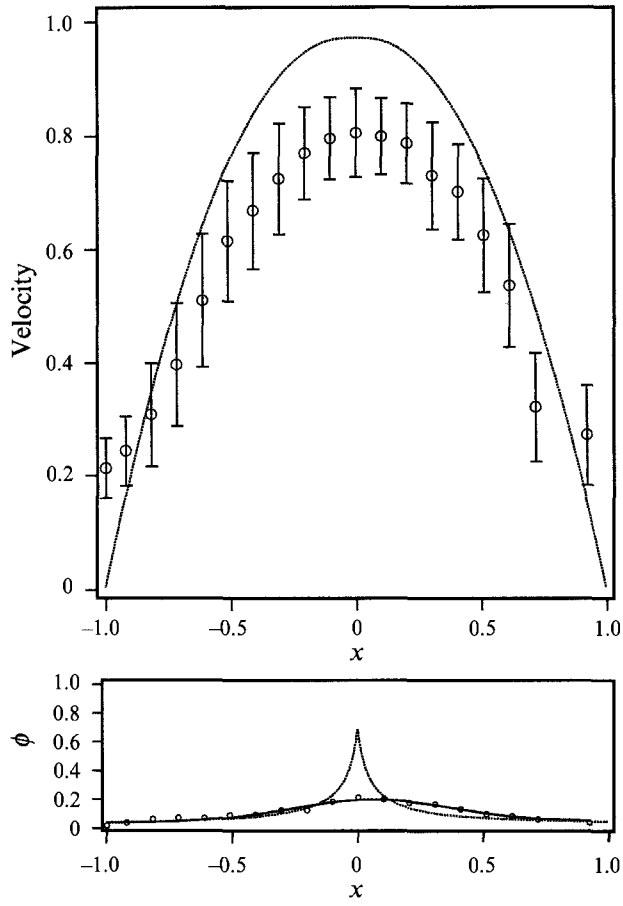

FIGURE 11. Velocity and concentration profiles for experiment 187 (see table 1): ○, data points; —, curve fits to data (see text); I, standard deviation for velocity data; ----, predictions from theory, §7. $Re_p = 2.0 \times 10^{-3}$; $\kappa = 0.019$; $\phi_{bulk} = 0.10$; $b = 2.05$.

Before discussing the data in figures 10–21, it is perhaps worth briefly discussing why the current data set is limited to volume fractions $\phi_{bulk} \leqslant 0.3$. This limitation actually exists for several reasons. First, the bulk viscosity of suspensions increases with particle concentration and we found that the syringe pump employed in our experiment could not provide a smooth flowrate at particle concentrations higher than 0.3. This has led us to replace the pump for future work with a model that is specifically intended for work with highly viscous fluids. Secondly, we did not observe (from the oscilloscope) distinct and well-defined Doppler bursts at higher particle concentrations. As explained earlier, it is necessary to allow the suspension to stand for a period of time so that any small bubbles created after stirring the suspension can rise to the top. We found that, for such high particle concentrations, an exceedingly long duration of standing time is required. Apparently, the quality of the refractive index match degrades beyond an acceptable level within this period for a high-concentration suspension. (For this same reason, we did not report any particle volume fraction profiles for the case of $\phi_{bulk} = 0.3$ and $\kappa = 0.010$ since we did not observe distinct Doppler bursts from the oscilloscope.) Current studies are exploring both new combinations of particles and suspending fluid, in which refractive indices of both phases remain constant, and also preparation procedures which minimize standing times after the final refractive index

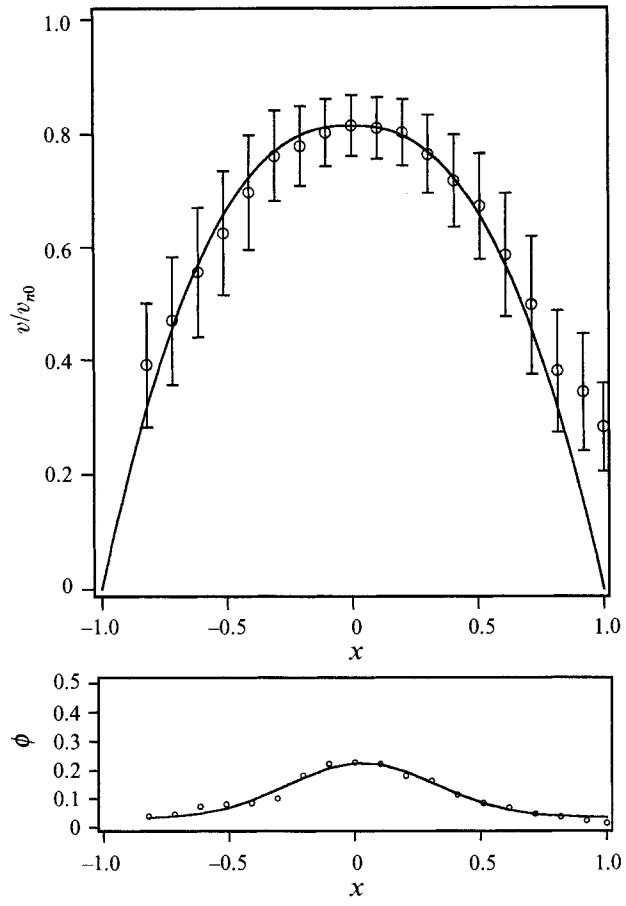

FIGURE 12. Velocity and concentration profiles for experiment 198 (see table 1): ○, data points; —, curve fits to data (see text); I, standard deviation for velocity data. $Re_p = 3.3 \times 10^{-3}$; $\kappa = 0.032$; $\phi_{bulk} = 0.10$; $b = 2.45$.

match is completed, with the intent of reducing this source of limitation on particle concentrations.

We will first discuss one specific set of data to highlight the general features. Figure 10 shows the particle velocity and volume fraction profiles for the case of $Re_p = 2.0 \times 10^{-3}$, $\kappa = 0.010$ and $\phi_{bulk} = 0.10$. On the top half of the figure, the ordinate is the particle velocity non-dimensionalized with $v_{n,0}$. The symbols (○) are the experimental data and the solid curve is the closest fit to the data using the form $v_z = v_{z,0}(1-|x|^b)$ that was first adopted by Kowalewski (1980). Here, $v_{z,0}$ is the centreline velocity, and the exponent b is treated as an adjustable parameter which we denote as the bluntness factor. It was noted earlier that the velocity data near the channel wall deviates slightly upward from the actual velocity owing to various limitations of the LDV set-up that was used. Although it is not entirely clear where this begins to have a significant impact on the averaged velocities reported here, we have (somewhat arbitrarily) ignored data for $|x| > 0.8$ when performing the least squares fit to determine b. Clearly, inclusion of data nearer to the walls would have led to larger values of the bluntness factor. The bottom half of figure 10 displays the particle volume fraction data. The solid line is obtained from a general curve fit of the data. The uncertainty in the volume fraction data is estimated to be about $\pm 10\%$ of its value. (Recall that these data are obtained

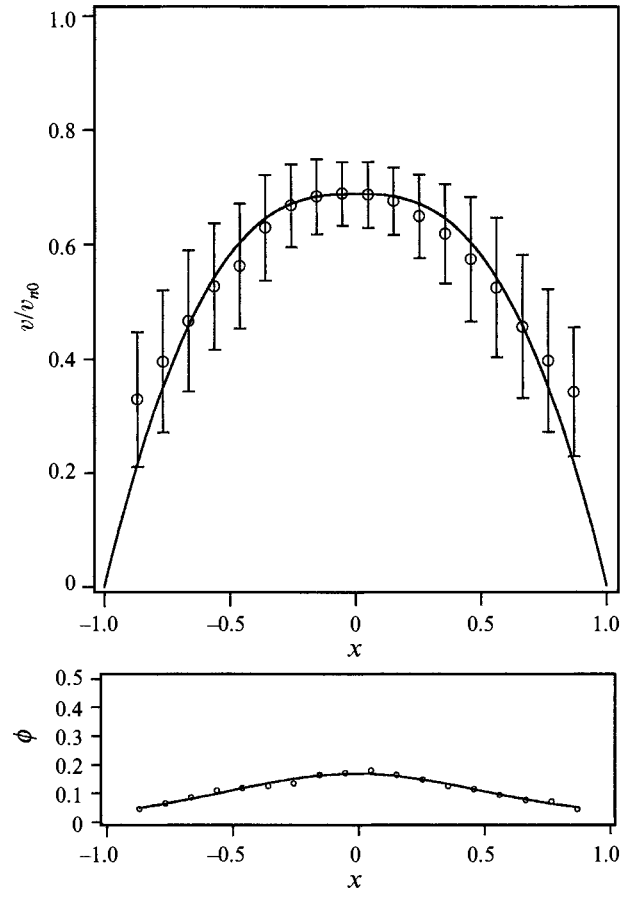

FIGURE 13. Velocity and concentration profiles for experiment 245 (see table 1): ○, data points; —, curve fits to data (see text); I, standard deviation for velocity data. $Re_p = 5.9 \times 10^{-3}$; $\kappa = 0.057$; $\phi_{bulk} = 0.10$; $b = 2.70$.

by measuring the time, $\Delta t(x)$, required to obtain a certain number of Doppler signals at position x in the flow channel. It is observed from the experiments that the volume fraction obtained from two consecutive sets of 1000 data points at the same location can differ by up to about 10%.)

In addition to the average velocity, we also report the standard deviation of the velocity. The magnitude of the standard deviation is determined by various effects. It is clear that the variation in velocity measured at each point in the flow channel is partially due to the velocity gradient within the finite-size measurement volume. However, in some cases the velocity profiles are highly blunted near the centre, which indicates the absence of any significant macroscopic velocity gradient. Thus, the presence of local velocity fluctuations in these cases should be due primarily to interactions (e.g. collisions) among the particles. In fact, it is these interactions (i.e. the irreversible collisions) that lead to the particle migration discussed in §1. Currently, we are in the process of obtaining other statistical information pertaining to the experiment. For example, in addition to velocity fluctuation, a time correlation of t_d (the time between successive valid Doppler signals, cf. §4.1) would provide a more detailed picture regarding the mechanisms of particle migration due to particle–particle interactions. We hope to report such results in a future paper.

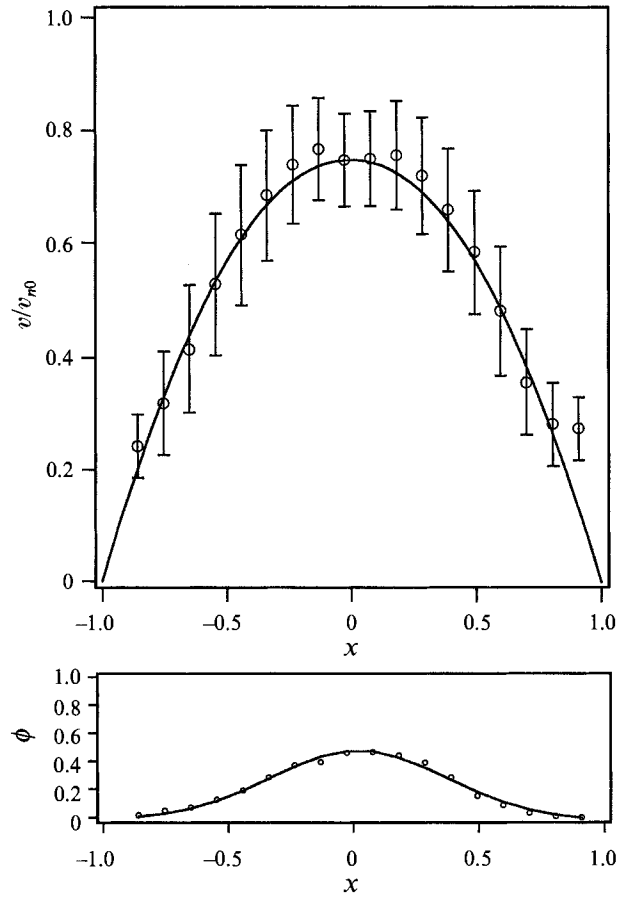

FIGURE 14. Velocity and concentration profiles for experiment 217 (see table 1): ○, data points; —, curve fits to data (see text); I, standard deviation for velocity data. $Re_p = 2.0 \times 10^{-3}$; $\kappa = 0.0120$; $\phi_{bulk} = 0.20$; $b = 2.05$.

To a large extent, the data represented in figures 10–21 speak for themselves, and, at the same time, it cannot be easily replaced in an abbreviated or consolidated form. We shall concentrate on the phenomena exhibited in these experiments with variations of the two parameters ϕ_{bulk} and κ.

The two most prominent features of the data are: (i) the non-uniformity of the concentration profiles, which exhibit a maximum value at the centreline and minimum values near the channel walls, and (ii) the blunting of the particle velocity profiles. The data shown in figures 10–21 allow one to independently assess the role of particle size (κ) and of the bulk concentration of particles ϕ_{bulk}.

First, for fixed values of κ, it is evident that the particle concentration profiles become increasingly non-uniform as ϕ_{bulk} is increased, and the velocity profiles also become increasingly blunted. The difference between the concentration profiles for $\phi_{bulk} = 0.1$, and the other two values for any fixed κ, may, in retrospect and with the advantage of the scaling argument of Nott & Brady (1993) to guide us, be a consequence of the fact that the measuring point is not far enough downstream from the entry for $\phi_{bulk} = 0.1$ to see the fully developed concentration profile. It may also be noted, in comparing the profiles for $\phi_{bulk} = 0.2$ and $\phi_{bulk} = 0.3$ that the peak (centreline) concentration in the latter case is getting relatively close to the maximum

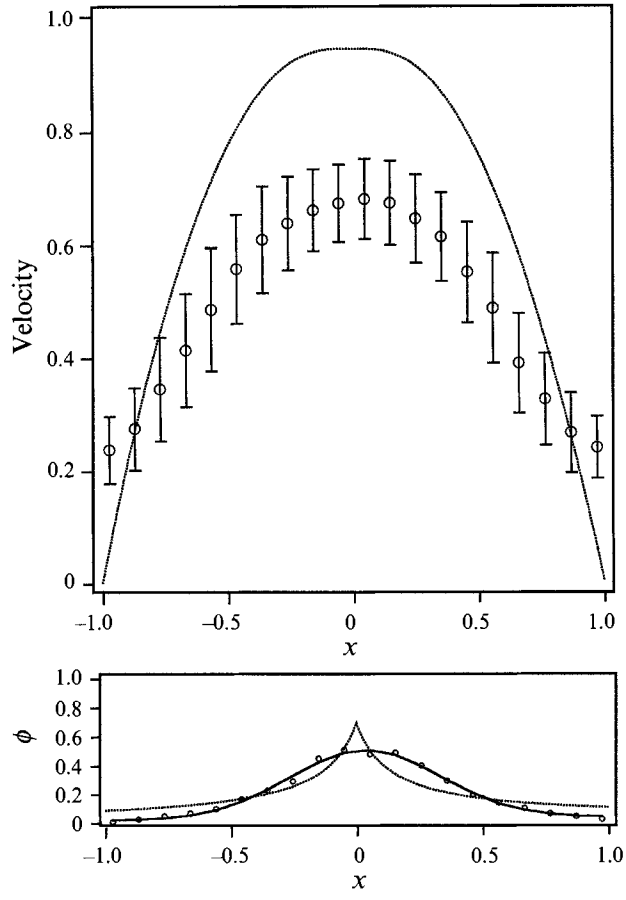

FIGURE 15. Velocity and concentration profiles for experiment 189 (see table 1): ○, data points; —, curve fits to data (see text); I, standard deviation for velocity data; -----, predictions from theory, §7. $Re_p = 2.0 \times 10^{-3}$; $\kappa = 0.019$; $\phi_{bulk} = 0.20$; $b = 2.30$.

allowable value, while that for $\phi_{bulk} = 0.2$ remains at a significantly lower value. This may be contrasted with the simple scaling theory of Leighton & Acrivos (1987) which, as we shall see, always leads to the conclusion that the centreline concentration should approach the maximum packing concentration. Although the significance is unclear to us at this time, another interesting fact is that the shape of the profiles for $\phi_{bulk} = 0.2$ and 0.3 is essentially the same once they are scaled with their centreline values. Most likely, this is simply coincidental. Certainly, if we were to continue to increase ϕ_{bulk} we would eventually reach more uniform concentration profiles with the limiting case being $\phi_{bulk} = \phi_{max}$ everywhere.

If we now examine the influence of particle size (namely κ) for fixed ϕ_{bulk}, we note that the concentration profiles for $\phi_{bulk} = 0.2$ and 0.3 are both completely independent of particle size (as the simple scaling theory predicts). Though this is not precisely true for $\phi_{bulk} = 0.1$, this may again be a result of making measurements too close to the entry region in that case. Obviously, with identical concentrations profiles for each value of ϕ_{bulk}, a simple continuum theory for the rheology, with $\mu^* = \mu(\phi)$ only, must predict that the velocity profiles for the various κ values should also be identical. However, this is not the case. As the particle size increases relative to the width of the channel, the velocity profiles become increasingly blunted and the maximum velocity

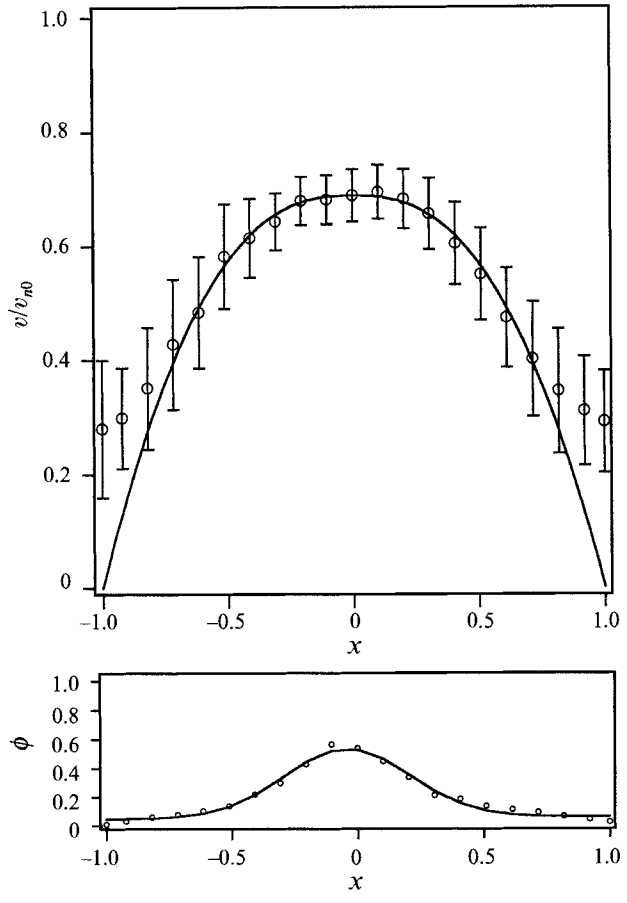

FIGURE 16. Velocity and concentration profiles for experiment 202 (see table 1): ○, data points; —, curve fits to data (see text); I, standard deviation for velocity data. $Re_p = 3.3 \times 10^{-3}$; $\kappa = 0.032$; $\phi_{bulk} = 0.20$; $b = 2.55$.

thus decreases. This is, in fact, clear evidence that a purely continuum theory cannot provide a full explanation of the observed behaviour. Looking back at the original measurements of Karnis *et al.* (1966), which were mentioned in §1, we see that their observation of blunted particle velocity profiles was also very strongly coupled to particle size: the strongest blunting occurred for the largest particles (0.0224 cm corresponding in their case to $\kappa = 0.057$); relatively little blunting was found for their smallest particles ($\kappa = 0.014$).

One additional feature of the present results should be mentioned here. As the particle concentration is increased from $\phi_{bulk} = 0.1$ to $\phi_{bulk} = 0.3$, there is a sharp reduction in the maximum particle velocity. This is, of course, not entirely unexpected. If the velocity and concentration profiles with both flat, the mean (and maximum) velocity would decrease to $\frac{2}{3}$ of its value for a parabolic velocity profile. Nevertheless, the measured particle velocities are lower than could be accounted for via modification of the shape of the velocity (and concentration) profiles, indicating a significant 'slip' between the particles and the suspending fluid which increases with increasing particle concentration and size. The numerical simulations of particle motion due to Nott & Brady (1993) do not show any slip between particles and the suspending fluid, and these authors suggest strongly that there should not be any relative motion between the

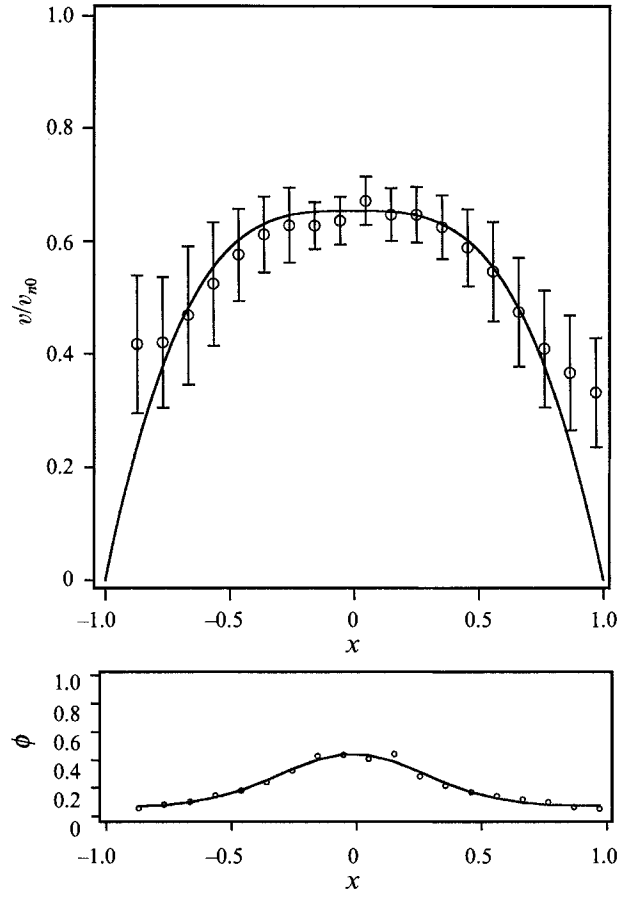

FIGURE 17. Velocity and concentration profiles for experiment 223 (see table 1): ○, data points; —, curve fits to data (see text); I, standard deviation for velocity data. $Re_p = 5.9 \times 10^{-3}$; $\kappa = 0.057$; $\phi_{bulk} = 0.20$; $b = 3.25$.

two phases (i.e. the particles and fluid).† Of course, the velocity of a single small particle will always be less than that of the fluid owing to interactions with the channel walls (cf. Happel & Brenner 1965; Kim & Karrila 1991), but the difference will be small, $O(a/d)$, for such a particle. We can offer no real explanation for our measured result at this time, except to suggest that the particles in a concentrated suspension may be in sufficiently close proximity that they can be considered as moving together as a larger body composed of a group of small particles. As indicated above, the lag in the particle velocity owing to wall effects increases as the particle size increases relative to the channel width. Clearly, it will be of interest in future studies to obtain independent data for both the particle and fluid phases, and this is quite possible by using a very low concentration of very small tracer particles that are optically distinct from the particles of the suspension.

† Owing to our own scepticism, based partially on similar reasoning, we have delayed returning this paper for publication in order to repeat many of the experiments as a check on our results. The experimental results obtained in these repeated experiments are indistinguishable within experimental uncertainty from the data reported here.

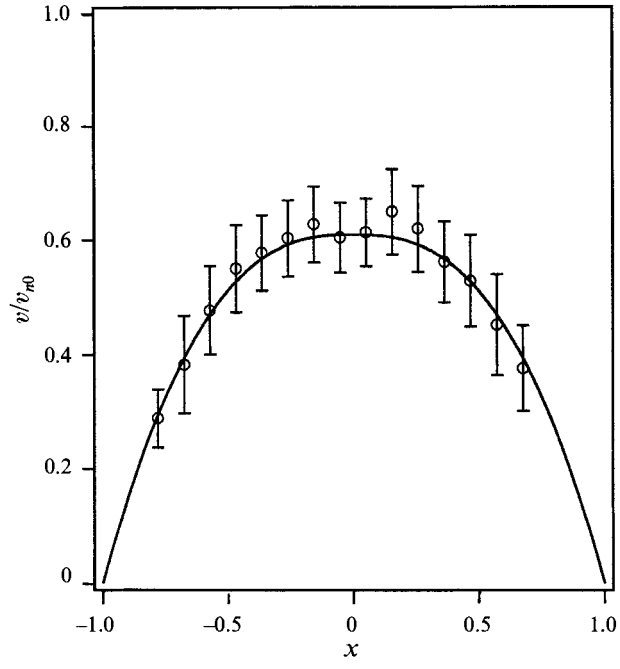

FIGURE 18. Velocity and concentration profiles for experiment 172 (see table 1): ○, data points; —, curve fits to data (see text); I, standard deviation for velocity data. $Re_p = 2.0 \times 10^{-3}$; $\kappa = 0.010$; $\phi_{bulk} = 0.30$; $b = 2.65$.

7. Comparison with theory

As mentioned in §1, there are three theoretical approaches that can be used to provide a basis for comparison with the present experimental data. Two of these, namely direct simulation via Stokesian dynamics, and the continuum theory of Nott & Brady (1993) have already been compared with our data in their forthcoming paper. Here, we limit our comparisons to the earlier scaling theory of Leighton & Acrivos as adapted by Phillips *et al.* (1992). Since the extension from cylindrical Poiseuille flow to rectangular channel flow is straightforward, we will simply state the basic ideas here and refer the reader to the paper of Phillips for more details. They assume that the suspension can be modelled as a generalized Newtonian fluid such that the deviatoric stress tensor

$$\tau = \eta(\phi)\,\dot{\gamma} \tag{26}$$

where $\dot{\gamma}$ is the rate-of-strain tensor and η is the viscosity. The dependence of the viscosity on the particle volume fraction is given by Krieger's empirical formula (1972)

$$\frac{\eta}{\eta_0} = \left(1 - \frac{\phi}{\phi_m}\right)^{-1.82} \tag{27}$$

where ϕ_m is the maximum packing volume fraction, assumed to be about 0.68.

Using the theory of Leighton & Acrivos, Phillips *et al.* derived the diffusion equation (1) for the particles. Applying this equation at steady state to the simple geometry of our problem (see figure 7), it is easy to show that

$$\frac{\dot{\gamma}\phi}{\dot{\gamma}_w \phi_w} = \left(\frac{\eta_w}{\eta}\right)^{K_\eta/K_c}. \tag{28}$$

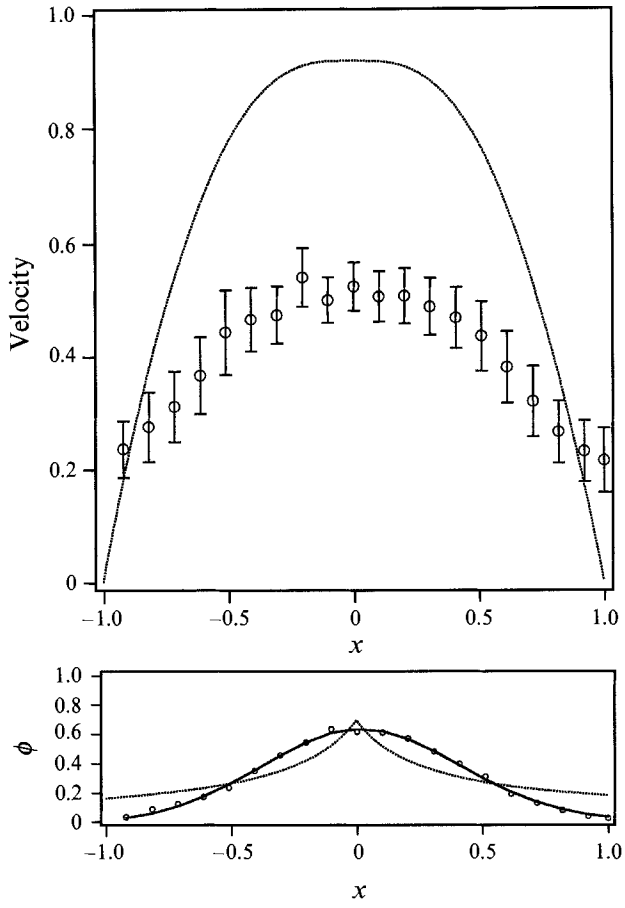

FIGURE 19. Velocity and concentration profiles for experiment 192 (see table 1): ○, data points; —, curve fits to data (see text); I, standard deviation for velocity data; -----, predictions from theory, §7. $Re_p = 2.0 \times 10^{-3}$; $\kappa = 0.019$; $\phi_{bulk} = 0.30$; $b = 2.60$.

Here, the subscript w refers to values evaluated at the wall and K_η and K_c are proportionality constants. From experimental data obtained from Couette flows, Phillips *et al.* (1992) found that $K_\eta/K_c = 0.66$.

Using the momentum equation and equation (26), we can show that

$$\dot{\gamma} = \frac{x}{\eta}. \tag{29}$$

Combining (28) and (29), and using the simplifying assumption that

$$1.82\ (1 - K_\eta/K_c) \mp -1,$$

we find

$$\phi = \frac{\phi_m}{1 + \alpha x}, \tag{30}$$

where

$$\alpha = \frac{\phi_m - \phi_w}{\phi_w}, \tag{31}$$

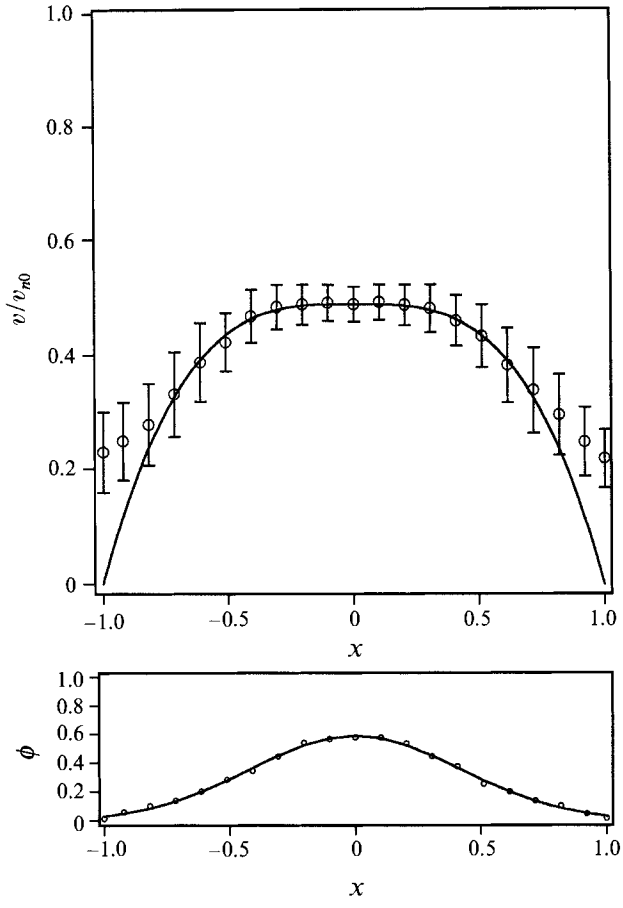

FIGURE 20. Velocity and concentration profiles for experiment 205 (see table 1): ○, data points; —, curve fits to data (see text); I, standard deviation for velocity data. $Re_p = 3.3 \times 10^{-3}$; $\kappa = 0.032$; $\phi_{bulk} = 0.30$; $b = 3.30$.

and it is related to the bulk volume fraction (ϕ_{bulk}) as

$$\phi_{bulk} = \int_0^1 \phi \, \mathrm{d}x$$

$$= \frac{\phi_m}{\alpha} \ln(1+\alpha). \tag{32}$$

Equation (30) predicts the particle distribution in the flow channel. Combining this equation with the momentum equation and Krieger's viscosity formula, we obtain

$$\frac{\mathrm{d}v}{\mathrm{d}x} = kx\left(\frac{x}{1+\alpha x}\right)^{1.82}. \tag{33}$$

Equation (33) is solved by the fourth-order Runge–Kutta method and k is a proportionality constant determined by the volumetric flowrate requirement

$$\int_0^1 v \, \mathrm{d}x = \tfrac{2}{3}. \tag{34}$$

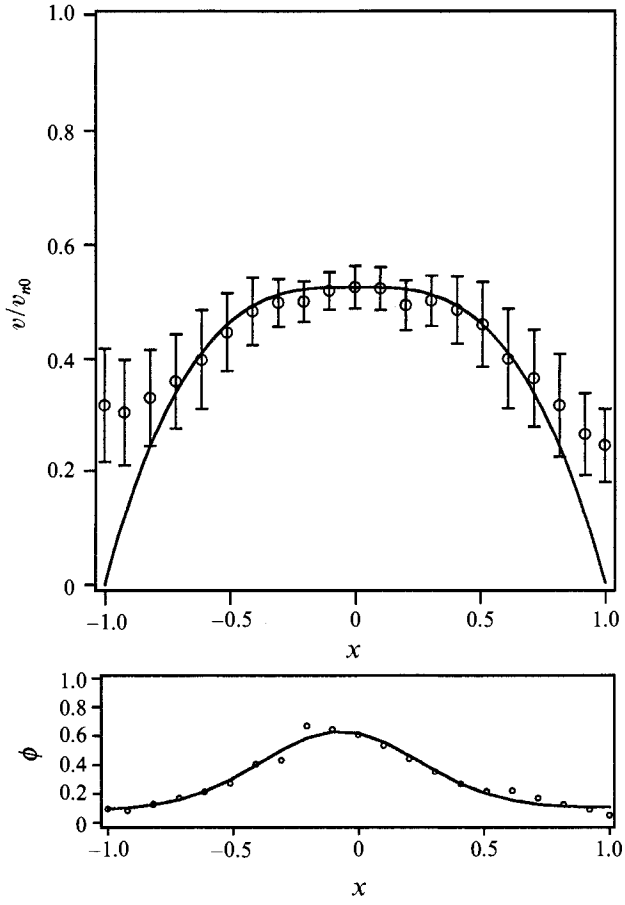

FIGURE 21. Velocity and concentration profiles for experiment 226 (see table 1): ○, data points; —, curve fits to data (see text); I, standard deviation for velocity data. $Re_p = 5.9 \times 10^{-3}$; $\kappa = 0.057$; $\phi_{bulk} = 0.30$; $b = 3.10$.

Two features of the model system may be commented upon immediately, as they are clearly at odds with the experiments. First, the theory is a continuum theory that regards the particles as points, so that the particle size does not directly enter either the governing equations, or the model predictions. In contrast, we have already seen that the particle size relative to the channel dimensions, as measured by κ, does seem to play a role in the experimental results. Secondly, and perhaps more importantly, the experiments indicate that the mean velocity of the particles at a point differs from that of the suspending fluid. In contrast, the theory treats the suspensions as a generalized Newtonian fluid and thus makes no allowance for any distinction between particle and fluid velocities.

A direct comparison between the theoretical predictions and the experimental data is included in figures 11, 15 and 19 for the three bulk particle concentrations ($\phi_{bulk} = 0.1$, 0.2 and 0.3) and one other arbitrarily chosen value of $\kappa = 0.019$. Specifically, the theoretical velocity profile, as calculated from (33) and the concentration profile given by (30) are shown in these figures as dotted lines. It is apparent that the velocity profiles do not agree with the experimental data, for reasons cited above. The concentration profiles, on the other hand, are more satisfactory, except for the immediate vicinity of the channel centreline. At this point, the theory

always predicts that ϕ equals the maximum value $\phi = 0.68$, thus disagreeing sharply with the measurements. This effect is a manifestation of characterizing the particles as points instead of finite size spheres. Since the shear rate, $\dot{\gamma}$, vanishes at the centre of the channel, the theory suggests that there are no particle collisions at this point, and thus no mechanism to oppose the diffusion toward this point. This unrealistic assumption can be improved with refinement of the theory to take account of the finite dimensions of the particles. By doing so, the theory would allow for particle collisions even when the shear rate vanishes; thus, there would still be an opposing flux at the centre of the flow channel. This would lead to a lower particle concentration near the centre and a particle concentration profile more similar to those obtained from experimental data.

To summarize, we find that the flow of concentrated suspensions in a rectangular channel is characterized by a blunting of the particle velocity profile. The magnitude of this blunting increases with increase of either the bulk particle concentration of the suspension or the ratio of the particle size to the gap width of the channel. We also find that the local particle concentration is not uniform across the gap of the flow channel; in general, the particles tend to concentrate near the centre of the flow channel. In fact, for certain instances (i.e. $\phi_{bulk} = 0.3$) the local particle concentration at the centreline approaches a 'maximum packing' value near 0.65. One of the most interesting phenomena inferred from this study is that there exists a relatively large slip velocity between the particle and the fluid, which increases as the bulk particle concentration increases. Consequently, it would appear to be important that any comprehensive theory for the flow of suspension should take this phenomenon into account. It is also clearly desirable to obtain direct measurements of the velocities of the suspending fluid, as well as the particles.

This work has been supported by a grant from the fluid mechanics and particulate processing programs of the National Science Foundation.

REFERENCES

ABBOT, J. R., TETLOW, N., GRAHAM, A. L., ALTOBELLI, S. A., FUKUSHIMA, E., MONDY, L. A. & STEPHENS, T. S. 1991 Experimental observations of particle migration in concentrated suspensions: Couette flow. *J. Rheol.* **35**, 773.

ADRIAN, R. J. 1978 Laser velocimetry. *T & MRep.* 442, University of Illinois, Dept of Theoretical and Applied Mechanics, Urbana, IL, USA.

ADRIAN, R. S. & EARLEY, W. 1976 Evaluation of LDV performance using Mie scattering theory. *Minnesota Symposium on Laser Anemometry Proceedings, Oct. 22–24, 1975, Bloomington, MN.* University of Minnesota, Dept of Conferences, Minneapolis.

CONAGHAN, B. F. & ROSEN, S. L. 1972 The optical properties of two-phase polymer systems: single scattering in monodisperse, non-adsorbing systems. *Polymer Engng Sci.* **2**, 12.

DRAIN, L. E. 1972 Coherent and noncoherent methods in Doppler optical beat velocity measurement. *J. Phys.* D *Appl. Phys.* **5**, 481.

DRAIN, L. E. 1980 *The Laser Doppler Technique.* John Wiley and Sons.

DURANI, T. S. & GREATED, C. A. 1977 *Laser Systems in Flow Measurements.* Plenum Press.

FAHRAEUS, R. & LINDQUIST, T. 1931 The viscosity of the blood in narrow capillary tubes. *Am. J. Physiol.* **96**, 562.

GADALA-MARIA, F. & ACRIVOS, A. 1980 Shear-induced structure in a concentrated suspension of solid spheres. *J. Rheol.* **24**, 799.

GAUTHIER, F., GOLDSMITH, H. L. & MASON, S. G. 1971 Particle motions in non-Newtonian media II. Poiseuille flow. *Trans. Soc. Rheol.* **15**, 297.

HAPPEL, J. & BRENNER, H. 1965 *Low Reynolds Number Hydrodynamics.* Prentice-Hall.

HOOKHAM, P. A. 1986 Concentration and velocity measurements in suspensions flowing through a rectangular channel. PhD thesis, California Institute of Technology.

JENKINS, J. T. & MCTIGUE, D. F. 1990 Transport processes in concentrated suspensions: the role of particle fluctuations. In *Two-Phase Flows and Waves*, ed. D. D. Joseph & D. G. Schaeffer, pp. 70–79. Springer.

JENKINS, J. T. & MCTIGUE, D. F. 1993 Viscous fluctuations and the rheology of concentrated suspensions. *J. Fluid Mech.* submitted.

KARNIS, A., GOLDSMITH, H. L. & MASON, S. G. 1966 The kinetics of flowing dispersions: I. concentrated suspension of rigid particles. *J. Colloid Sci.* **22**, 531.

KARNIS, A. & MASON, S. G. 1967 Particle motions in sheared suspensions. XIX. Viscoelastic media. *Trans. Soc. Rheol.* **10**, 571.

KIM, S, & KARRILA, S. J. 1991 *Microhydrodynamics*. Butterworth-Heinemann, Boston, MA.

KOH, C. J. 1991 Experimental and theoretical studies on two-phase flows. PhD thesis, California Institute of Technology.

KOWALEWSKI, T. A. 1980 Velocity profiles of suspension flowing through a tube. *Arch. Mech.* **32**, 857.

KOWALEWSKI, T. A. 1984 Concentration and velocity measurements in the flow of droplet suspensions through a tube. *Exps Fluids* **2**, 213.

KOWALEWSKI, T. A. 1987 An experimental study of the lateral migration of a droplet in a creeping flow. *Exps Fluids* **5**, 43.

KRIEGER, I. M. 1972 Rheology of monodisperse lattices. *Adv. Colloid Interface Sci.* **3**, 111.

LEAL, L. G. 1980 Particle motions in a viscous fluid. *Ann Rev. Fluid Mech.* **12**, 435.

LEIGHTON, D. & ACRIVOS, A. 1987 The shear-induced migration of particles in concentrated suspensions. *J. Fluid Mech.* **181**, 415.

MCMAHON, T. A. & PARKER, R. R. 1975 Particles in tube flow at moderate Reynolds number. *Trans. Soc. Rheol.* **19**, 445.

NOTT, P. R. & BRADY, J. F. 1993 Pressure-driven flow of suspensions: simulations and theory. *J. Fluid Mech.* submitted.

NOURI, J. M., WHITELAW, J. H. & YIANNESKIS, M. 1986 An investigation of refractive-index matching of continuous and discontinuous phases. *Third Intl Symp. on Applications of Laser Anemometry to Fluid Mech.* Portugal.

PHILLIPS, R. J., ARMSTRONG, R. C., BROWN, R. A., GRAHAM, A. & ABBOT, J. R. 1992 A constitutive equation for concentrated suspensions that accounts for shear-induced particle migration. *Phys. Fluid* A **4**, 30.

SEGRÉ, G. & SILBERBERG, A. 1962 Behaviour of macroscopic rigid spheres in Poiseuille flow. Parts 1 and 2. *J. Fluid Mech.* **14**, 115, 136.

SEGRÉ, G. & SILBERBERG, A. 1963 Non-Newtonian behavior of dilute suspensions of macroscopic spheres in a capillary viscometer. *J. Colloid Intl Sci.* **18**, 312.

SINTON, S. W. & CHOW, A. W. 1991 NMR flow imaging of fluids and solid suspensions in Poiseuille-flow. *J. Rheol.* **35**, 735.

TIMMERMANS, L. 1965 *Physico-Chemical Constants of Pure Organic Compounds*, Vol. 2. Elsevier.

VAN DE HULST, H. C. 1957 *Light Scattering by Small Particles*. Wiley.